Journal Pre-proof

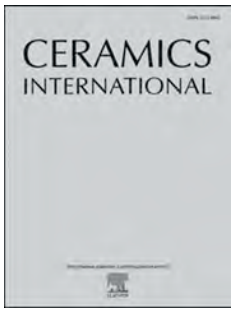

Dielectric relaxation behavior of $BaZrO_3$ ceramics at low temperature

Phieraya Pulphol, Naratip Vittayakorn, Wanwilai Vittayakorn, Taras Kolodiazhnyi

PII: S0272-8842(20)31894-0

DOI: https://doi.org/10.1016/j.ceramint.2020.06.234

Reference: CERI 25661

To appear in: *Ceramics International*

Received Date: 1 April 2020

Revised Date: 2 June 2020

Accepted Date: 20 June 2020

Please cite this article as: P. Pulphol, N. Vittayakorn, W. Vittayakorn, T. Kolodiazhnyi, Dielectric relaxation behavior of $BaZrO_3$ ceramics at low temperature, *Ceramics International* (2020), doi: https://doi.org/10.1016/j.ceramint.2020.06.234.

Dielectric relaxation behavior of $BaZrO_3$ ceramics at low temperature

Phieraya Pulphol[1,2], Naratip Vittayakorn*[1,2], Wanwilai Vittayakorn[1,2]

and Taras Kolodiazhnyi[4]

[1]Electroceramic Research Laboratory, College of Nanotechnology, King Mongkut's Institute of Technology Ladkrabang, Bangkok 10520, Thailand

[2]Advanced Material Research Unit, Faculty of Science, King Mongkut's Institute of Technology Ladkrabang, Bangkok 10520, Thailand

[3]National Institute for Materials Science, 1-1 Namiki, Tsukuba, Ibaraki 305-0044, Japan

Abstract

Dielectric behavior of nominally pure $BaZrO_3$, Sc-doped $BaZrO_3$ and Sc+Nb-co-doped $BaZrO_3$ ceramics is reported in this paper. Several dielectric anomalies are detected in the pure and Sc-doped $BaZrO_3$ in temperature interval of 2-700 K. The Arrhenius-type dielectric relaxation has activation energies ranging from ca. 10 meV to 800 meV. Annealing in Ar atmosphere at 1200°C alters the intensity of the dielectric loss peaks especially in the Sc-doped $BaZrO_3$. In contrast, none of the dielectric relaxation anomalies were found in Sc+Nb-co-doped $BaZrO_3$. It is proposed that at least some of the dielectric peaks originate from the proton dynamics which includes high temperature migration, intermediate-temperature rotation and low-temperature phonon-assisted proton tunneling.

Keywords: Dielectric anomalies; Barium zirconate; Phonon-assisted proton tunneling

*Corresponding author, E-mail: naratip.vi@kmitl.ac.th

1. Introduction

Although less popular than $BaTiO_3$, $BaZrO_3$ (BZ) is one of the widely studied perovskite ceramics [1]. Structural studies of BZ suggest a simple cubic perovskite structure with no apparent phase transition in the temperature range of 2-1700 K [2]. Because of its excellent refractory properties BZ has been used as a Tamman tube to grow high Tc superconducting single crystals. Also, BZ is an additive material for ceramic capacitors and microwave dielectric resonator ceramics. When doped with proper acceptor impurities, such as Y^{3+}, Sc^{3+}, Gd^{3+}, etc. [3-6] and annealed in humid atmosphere, BZ shows remarkable protonic conductivity above 500 C and is a promising material for proton-conducting fuel cells and proton electrochemical reactors and sensors [7-9].

There are numerous works on the dielectric and proton conducting properties of $BaZrO_3$ at room or high temperature. However, in many perovskites, the unusual dielectric phenomena are known to occur at very low temperatures (T < 50 K). The low temperature behavior of $BaZrO_3$ is still poorly understood. The structural study of $BaZrO_3$ using X-ray and neutron diffraction shows that $BaZrO_3$ possesses cubic symmetry down to 2 K [10]. The first-principles studies are somewhat in conflict with the diffraction data. According to [11-12], the low symmetry structural instability in $BaZrO_3$ occurs at the R- and M-points. Moreover, the evidence of the short-range low symmetry distortions is well supported by the experimental results from far-infrared, THz-TDS and Raman spectroscopy [13-14].

The first report on the low temperature dielectric properties of $BaZrO_3$ has appeared in Ref.10. According to Ref 10, the real part of the dielectric permittivity (ε') of $BaZrO_3$ increases as the temperature decreases and follows incipient ferroelectric behavior. The overall increase in ε' with decreasing temperature is similar to that found in other incipient

ferroelectrics, such as $KTaO_3$ and $SrTiO_3$, where zero-point quantum effects result in the low-T dielectric behavior that follows the Barrett equation,

$$\varepsilon' = \frac{C}{T_S coth\left(\frac{T_S}{T}\right) - T_0} + B, \quad (1)$$

where C is the Curie constant, T_S is saturation temperature, T_0 is the classical Curie temperature and B is a temperature independent constant. However, unlike $KTaO_3$ and $SrTiO_3$ quantum paraelectrics [15-16], $BaZrO_3$ shows strongly negative T_0 similar to $EuTiO_3$ and $CaTiO_3$ incipient ferroelectrics [17-18]. The two humps in $\varepsilon'(T)$, are proposed to originate from the oxygen octahedra rotation (at $T \approx 15$ K) and the dipolar relaxation of extrinsic defects (at $T \approx$ 50-65 K) [10].

Recently, we studied dielectric properties of several BZ ceramics including undoped $BaZrO_3$, donor-doped ($BaZr_{0.995}Nb_{0.005}O_3$), acceptor-doped ($BaZr_{0.99}Ga_{0.01}O_3$) and the (1-$x$) $BaZrO_3$-$x BaGa_{0.5}Nb_{0.5}O_3$ solid solution [19]. Several dielectric relaxation peaks were detected in the undoped and acceptor-doped samples. Surprisingly, these peaks were suppressed in Nb-doped ceramics as well as in the $BaZrO_3$-$BaGa_{0.5}Nb_{0.5}O_3$ solid solutions. The origin of the dielectric relaxation peaks was attributed to the extrinsic impurities and relaxation dynamics of proton interstitials in $BaZrO_3$. The understanding of the correlation between these dielectric anomalies and defect chemistry may be important to solve practical application issues in the future devices.

In this work, the dielectric behavior of $BaZrO_3$, $BaZr_{1-x}Sc_xO_{3-x/2}$ and $BaZr_{0.98}Sc_{0.009}Nb_{0.011}O_3$ is examined in detail. Several dielectric relaxation peaks are detected in a wide temperature range ($2 < T < 700$ K). The effects of annealing in Ar atmosphere on the dielectric properties of doped- and undoped $BaZrO_3$ are discussed.

2. Experimental procedure

The $BaCO_3$, ZrO_2, Sc_2O_3 and Nb_2O_5 powders were used as starting materials. They were weighed to achieve a target composition of $BaZrO_3$, $BaZr_{1-x}Sc_xO_{3-x/2}$ (where x = 0.01 and 0.02) and $BaZr_{0.98}Sc_{0.009}Nb_{0.011}O_3$. All systems were synthesized via solid state reaction by ball-milling in ethanol for 20 hours then drying and compacting with 25 mm diameter WC pressing die. The pucks were calcined at 1300°C for 10 hours in air. The calcined samples were crashed and re-milled, then dried at 60˚C overnight. The powders were mixed with 5% PVA (polyvinyl alcohol) as a binder and pelletized into disks of 7 mm diameter and 1-2 mm thickness under 100 MPa uniaxial pressure. The green bodies were sintered at 1650°C for 20 hours in air. To study the defect mechanism, the sintered samples were annealed in Ar atmosphere at 1200°C for 20 hours and the silver ink electrodes were applied in the Ar glove box to avoid exposure to ambient atmosphere. The powder X-ray diffraction (Rigaku Miniflex600 X-ray diffractometer) with Cu K_α X-ray source (λ = 0.154185 nm, 2θ = 10-100 degrees) was used to study the phase composition of sintered ceramics. The lattice parameters were obtained from Le Bail refinement using JANA2006 software. The relative density (ρ) of sintered ceramics was calculated from the theoretical and experimental densities. The microstructure of the ceramics was studied by FE-SEM (Model S-4800 FE-SEM). The dielectric properties were investigated by PPMS Model 6000 (Physical Property Measurement System, Quantum Design, USA) and Impedance Analyzer (Novocontrol Technologies, Germany) at 2-360 K in the frequency range from 10 Hz-500 kHz. The dielectric properties at temperature of 300- 700K were studied using Agilent LCR meter in the frequency range from 10 Hz-1 MHz. The proton concentration was estimated from the weight loss of the powder samples using a thermogravimetric analysis (TGA, Pyris 1, PerkinElmer) under N_2 gas atmosphere from room temperature to 900˚C.

3. Results and discussions

3.1 X-ray diffraction (XRD)

The X-ray diffraction patterns of 99%, 99.9% and 99.99% pure $BaZrO_3$ (abbreviated as 2N, 3N and 4N, respectively) and doped $BaZrO_3$ (1%Sc and 2%Sc) sintered at 1650˚C for 20 hours are illustrated in Figure 1. The relative density of all sintered samples is more than 90% of the theoretical density value. The undoped samples as well as 2%Sc-doped samples show phase pure perovskite structure without any unknown phases detected. For 1%Sc-doped $BaZrO_3$, traces of second phase are detected at 2θ around 24 degree which corresponds to $BaCO_3$ phase. This is probably due to small errors during sample preparation. The XRD patterns of all systems are verified as cubic perovskite (space group *Pm-3m*) using Le Bail refinement software and are in good agreement with the standard file from the Inorganic Crystal Structure Database (ICSD) code 90049.

The lattice parameters obtained from the refinement are summarized in Table 1. For undoped systems (2N, 3N and 4N), the average lattice parameter (*a*) = 4.1943(2) Å is in agreement with other study [20] for pure $BaZrO_3$. Doping $BaZrO_3$ with trivalent ion such Sc causes a slight change in the lattice parameter. The lattice parameter (*a*) of Sc-doped $BaZrO_3$ tends to be a little larger than that of pure $BaZrO_3$. Because the ionic radius of Zr^{4+} is 0.72 Å, the substitution of Sc^{3+} ion with ionic radius of 0.745 Å on Zr^{4+}-site results in a slightly larger lattice parameter (*a*).

3.2 Scanning electron microscope (SEM) analysis

The SEM microstructures of doped- and undoped-$BaZrO_3$ samples are illustrated in Figure 2. Among undoped systems, BZ 3N shows the smallest grain size with rather poor density (~90%) whereas BZ 2N shows the highest density of ~98%. The average grain size of undoped samples are 2.5(3) μm, 1.8(4) μm and 3.2(4) μm for BZ 2N, BZ 3N and BZ 4N, respectively. Figure 2(d-e) shows the effect of the Sc additive. As seen from the figure, doping 1% Sc provides 1.4(6) μm of average grain size and the grain size is further decreased

when the amount of scandium increases to 2% (0.7(4) μm). From the results it can be assumed that scandium inhibits grain growth and leads to the smaller grain size.

3.3 Dielectric properties

The dielectric properties of sintered samples were investigated from 360 K down to 2 K at frequency f = 10 Hz-500 kHz. Figure 3(a) shows the dielectric permittivity and tan δ at 1 kHz of the undoped BZ samples (2N, 3N and 4N) sintered in air. The room temperature ε' is around 38, 33 and 39 for BZ 2N, 3N and 4N, respectively, which agrees with other studies [10,21]. The ε' increases upon cooling. This behavior is similar to other incipient ferroelectrics such as $CaTiO_3$ and $EuTiO_3$ [17,22]. It is also similar to the low temperature dielectric simulation study of Akbarzadeh et al. that shows that the quantum fluctuations affect the dielectric behavior of pure $BaZrO_3$ [10]. Figure 3(b) shows the low temperature behavior of ε' of BZ 3N. Several dielectric anomalies in the form of ε' humps and tan δ peaks can be detected in our $BaZrO_3$ samples, as reported earlier [19]. We assume that the ε' humps at around 3-5K result from the oxygen octahedra rotation as proposed in Ref. [10]. As seen from Figure 3(a), several dielectric anomalies occur in undoped $BaZrO_3$. The tan δ of BZ 2N, 3N and 4N from 2 K to 360 K is shown in Figure 4(a). The low-temperature details of the tan δ behavior in the 2-200K range are shown in Figure 4(b). Several tan δ peaks appear at around 11 K < T < 160 K labeled as T_1, T_2, T_3 and T_4 in Figure 4(b). They shift to higher temperature as frequency increases. The similar trend is found in Sc-doped $BaZrO_3$. Four peaks in 1% and 2% Sc-doped $BaZrO_3$ at 18 K, 40 K, 96 K and 122 K indexed as T_1, T_2, T_3 and T_4, respectively, are detected in Figure 5(b). The tan δ peaks of 1% and 2% Sc-doped BZ occur at almost the same temperature and the tan δ peak magnitude at T > 50K increases with the Sc concentration.

To further study the origin of the low temperature dielectric anomalies, we annealed all the samples in Ar atmosphere and the results of dielectric loss peaks and their Arrhenius behavior are presented in Figures 5(a) and 6. The low-temperature loss peaks (at T < 100K) of undoped BZ seem to be little affected by the anneal in Ar as they appear at the same temperature for both samples sintered in air and annealed in Ar (see Fig 6(a)). In contrary to undoped BZ, the loss peaks at around 96 K and 122 K for the Sc-doped samples almost vanish after annealing in Ar (see Fig 5(a)). The activation energies of these loss peaks were obtained from Arrhenius type behavior:

$$f = f_0 exp\left(\frac{-E_a}{k_B T_{max}}\right), \quad (2)$$

where E_a is the activation energy, k_B is Boltzmann constant, T_{max} is the temperature of the tan δ maximum and f_0 is a constant. The calculated activation energies are summarized in Table 2 for undoped BZ. The activation energies of dielectric relaxation ranging from 0.016 to 0.276 eV are almost the same for both air-sintered and Ar-annealed undoped BZ (Table 2). The activation energies of dielectric relaxation of Sc-doped BZ are shown in Table 3. While the dielectric relaxation with E_a = 0.026-0.031 eV persist in both as-sintered and Ar-annealed Sc-doped BZ, the dielectric relaxation processes with E_a = 0.057-0.175 eV almost vanish after annealing in Ar. We suggest, therefore, that the dielectric anomalies with E_a = 0.057-0.175 eV are most likely associated with the localized motion of the protons.

It is well known that doping $BaZrO_3$ with acceptor impurities, such as trivalent ions, leads to the formation of oxygen vacancies according to:

$$M_2O_3 \rightarrow 2M'_{Zr} + V_O^{\bullet\bullet} + 3O_O^{\times}, \quad (3)$$

where M is the trivalent ion, $V_O^{\cdot\cdot}$ is oxygen vacancy and $O_O^{\times}$ is oxygen at oxygen site. Hereafter the Kröger-Vink notation is used for point defects. Nominally pure $BaZrO_3$ may still contain intrinsic acceptor impurities in the form of Ba-vacancies which naturally occur during

sintering at high temperatures due to loss of Ba. When exposed to humid atmosphere, the incorporation of protons occurs in the form of hydroxyl group (OH^-) that fill up the oxygen vacancies [23-24] according to:

$$H_2O + O_O^{\times} + V_O^{\bullet\bullet} \leftrightarrow 2OH_O^{\bullet} \quad (4)$$

From the Eq.4, the two OH^- groups form after the reaction between a water molecule with an oxygen vacancy. The protonic defect can migrate from one oxygen ion to the other ion, resulting in itinerant proton conductivity. $BaZrO_3$ is a well-known proton conductor at intermediate temperature with activation energy of proton migration of around 0.5-0.6 eV [25].

At low temperature, it is possible that the dielectric anomalies are produced by protonic defects. Several dielectric peaks indicate several types of proton motion with different activation energies. The DFT calculations have mapped several proton migration paths in $BaZrO_3$ doped with different kinds of dopant (e.g. Ga, Sc, In, Y and Gd) [6]. In the perovskite materials, there are two possible pathways for the classical proton motion: (i) proton transfer between the oxygen site of the adjacent lattice and (ii) the reorientation of proton at the oxygen site [6]. According to various estimates, the energy for proton transfer (E_{trans}) is in the range of 0.13-0.2 eV whereas the energy for the reorientation (E_{re}) is around 0.2 eV [6]. The activation energies of the low temperature dielectric anomalies T_2, T_3 and T_4, are in the range of 0.04-0.22 eV. It is possible that the origin of the low-energy dielectric anomalies comes from the localized reorientation and transfer of proton in the vicinity of the acceptor ions or other defects. The vanishing of the dielectric anomalies with E_a = 0.057-0.175 eV in the Sc-doped BZ annealed in Ar (i.e., in low water pressure atmosphere) well supports this conclusion.

The high temperature dielectric and Arrhenius behavior of undoped- and doped- $BaZrO_3$ (T > 250K) are illustrated in Figs 7 and 8. It was reported that the migration energy of proton conduction is around 0.5 eV in $BaZrO_3$ [25]. This energy is very close to the activation energy in our study (E_a =0.53-0.82 eV). Therefore, the high temperature relaxation could be attributed to the itinerant protonic defects and these peaks disappear after annealing in Ar atmosphere.

Several dielectric peaks at 13 K < T < 70 K in undoped and Sc-doped $BaZrO_3$ seem to be less sensitive to annealing in Ar and are more difficult to decipher (see Figs 3, 4, 5, 6). They may be attributed to the extrinsic impurities, as originally proposed in Ref. 10. In other oxides it has been reported that the low temperature tan δ peaks appear at the temperature range of interest (T < 100 K) and can be induced by defects or oxygen vacancies [26-28]. In $KTaO_3$ [26], doping with other ions such as Nb, Na and Fe causes low temperature dielectric anomalies induced by some defects located near oxygen vacancies. The 'rattling' ions with smaller ionic radii than the host ion is reported in Mn-doped $SrTiO_3$, $BaMg_{1/3}Ta_{2/3}O_3$ and Li-doped $KTaO_3$ [29-32]. In n-type $BaTiO_3$ or reduced $BaCeO_3$ the similar dielectric anomalies have been attributed to trapped excess electrons called "*polarons*" with an activation energy of 0.06-0.08 eV [26-28,33-34]. In addition to being a proton conductor, it is possible that hole conductivity can take place in the BZ as reported in several experimental studies [35-37]. Impurities from the processing (e.g. Cr^{3+}, Fe^{3+}, Al^{3+}) or intentional additives (e.g. Gd^{3+}, Y^{3+}, Sc^{3+}) are compensated by oxygen vacancy (as seen in Eq. 3). In dry atmosphere, holes can form in acceptor-doped $BaZrO_3$. Ref. [37] proposed two characteristics of hole, which are, (i) delocalized (free) hole polaron and (ii) bound hole polaron as seen in Eq. 5-6.

$$\frac{1}{2}O_2(g) + V_O^{\bullet\bullet} + O_O^{\times} \leftrightarrow 2h^{\bullet} + 2O_O^{\times} \quad (5)$$

$$\frac{1}{2}O_2(g) + V_O^{\bullet\bullet} + O_O^{\times} \leftrightarrow 2O_O^{\bullet} \quad (6)$$

where $V_O^{\cdot\cdot}$ is oxygen vacancy, $O_O^{\times}$ is oxygen at oxygen site, $h^{\bullet}$is a free hole polaron and $O_O^{\bullet}$ is a bound hole polaron at oxygen site. The activation energy of the hole migration is in the range of 0.4-0.8 eV [40]. At low temperatures, the localized motion of trapped holes may contribute to the dielectric relaxation detected in this study.

It is noteworthy that in our previous study the dielectric anomalies were completely suppressed by doping $BaZrO_3$ with donor ions, such as Nb^{5+} [19]. Donor ions compensate accidental (or intentional) acceptor impurities and expel oxygen vacancies. As a result, both the protonic defects and the oxygen vacancies can be eliminated by doping BZ with donor ions. To explore this scenario, we charge compensate Sc^{3+} by Nb^{5+} according to the formula $BaZr_{0.98}Sc_{0.009}Nb_{0.011}O_3$. In this formula we have used a very small excess of Nb (e.g., 0.2%) to charge compensate possible accidental acceptor impurities. Remarkably, the dielectric behavior of $BaZr_{0.98}Sc_{0.009}Nb_{0.011}O_3$ shows the complete elimination of the dielectric anomalies at low temperature as seen in Fig 9.

Since the estimated activation energies of both proton and electron hole conductivity are quite similar in the studied temperature range it is not easy to distinguish between these two types of defects. To bring clarity to this issue we applied the TGA analysis which favors the protonic defects. The weight loss of the selected samples determined from the TGA measurements are represented in Fig 10. The overall weight loss of 2%Sc doped sample is approximately 0.29%. This is due to the release of water as the temperature is increased to 900˚C. The ~0.18% weight loss that occurred from room temperature to around 400˚C comes from the water adsorbed on the surface of the powder sample. A more step weight loss of ~0.11% occurs at 400˚C – 800˚C and is qualitatively similar to the one reported in 10% Sc doped $BaZrO_3$ reported in [38-39]. This weight loss is attributed to the water released from the bulk of the crystal lattice and is in reasonable agreement with 0.056% weight loss expected for 2% Sc doped $BaZrO_3$. In contrast, the Sc-Nb doped $BaZrO_3$ sample shows

around 0.05% weight loss that mostly occurs below 400 C and attributed to adsorbed water as seen from Fig 10. This supports our hypothesis that Nb doping expels oxygen vacancies (and protonic defects) from the lattice of $BaZrO_3$.

Finally, we would like to bring the reader's attention to the very interesting results reported in Ref. 40. The quasielastic neutron scatting data indicate a very low energy (i.e., 0.01-0.03 eV) of proton dynamics in $BaZr_{0.90}A_{0.10}O_3$ (A = Y and Sc) [40]. To reconcile this energy with the other literature data on proton dynamics in BZ, the authors suggested that the classical barrier for proton transfer can be effectively reduced to 10-30 meV by the zero-point effect [40]. It is remarkable that our dielectric relaxation (i.e., dielectric peak T_1 with E_a = 16-31 meV) data are in very good agreement with the quasielastic neutron scatting data of Sc- and Y-doped BZ [40]. Here we would like to stress that, in addition to the zero-point effect; another effect such as the phonon-assisted proton tunneling may also result in such a low-energy proton dynamic, as proposed theoretically by Sundell et. al. [41]. It is interesting that in the case of BZ, the energy required to assist the proton tunneling can be supplied not only by acoustic phonons but also by the soft optical phonon mode with the energy of 15 meV as revealed by the terahertz spectroscopy [14].

4. Conclusion

We studied the dielectric anomalies in undoped- and doped-$BaZrO_3$. Several dielectric loss peaks associated with dielectric relaxation appear in the temperature range of 5 K – 700 K. The thermogravimetric results show the existence of water in the lattice (protonic defects) in acceptor-doped $BaZrO_3$. We assume that most of these dielectric anomalies are probably due to the proton dynamics. The high temperature dielectric peaks above 400 K are due to the itinerant proton transport with the activation energy of 0.5-0.8 eV. At $100 < T < 200$ K, protons become localized near acceptor impurities and contribute to the

localized proton dynamics with energies of 0.05-0.2 eV. The possible mechanisms for the proton motion are: (i) proton transfer between the oxygen site of the adjacent lattice and (ii) the reorientation of proton at the oxygen site. We propose the two possible origins for the lowest dielectric anomalies (T_1) which may be the zero-point energy or the phonon-assisted proton tunneling. The proton defects in our experimental finding can be partially eliminated by annealing in Ar (i.e., at low water partial pressure); however, we find that doping with donor ions such as Nb, is more effective in protonic defect suppression.

Acknowledgement

P.P. was supported by KMITL for PhD scholarship and internal NIMS projects PA5160 and PA4020. The work of N.V. was funded by King Mongkut's Institute of Technology Ladkrabang under grant KREF146201. N.V. and T.K. acknowledge the KMITL "Academic Melting-Pot" program under grant no. KREF206203.

References

[1] J.W. Bennett, I. Grinberg and A.M. Rappe, Effect of symmetry lowering on the dielectric response of $BaZrO_3$, Phys. Rev. B. 73 (2006) 180102 (1-4).

[2] G. Taglieri, G. Tersigni, P.L. Villa, C. Mondelli, Synthesis by the citrate route and characterization of $BaZrO_3$, a high-tech ceramic oxide: preliminary results, Int. J. Inorg. Mater> 1 (1999) 103.

[3] N. Kitamura, J. Akola, S. Kohara, K. Fujimoto and Y. Idemoto, Proton distribution and dynamics in Y- and Zn-doped $BaZrO_3$, J. Phys. Chem. 118 (2014) 18846-18852.

[4] H. Takahashi, I. Oikawa and H. Takamura, Atomistic insight into the correlation among oxygen vacancies, protonic defects, and acceptor dopants in Sc-doped $BaZrO_3$ using first-principles calculations, J. Phys. Chem. 122 (2018) 6501-6507.

[5] I. Ahmed, S.-G. Eriksson, E. Ahlberg, C.S. Knee, H. Götlind, L.-G. Johansson, M. Karlsson, A. Matic and L. Börjesson, Structural study and proton conductivity in Yb-doped BaZrO3, Solid State Ionics 178 (2007) 515-520.

[6] M.E. Björketun, P.G. Sundell and G. Wahnström, Structure and thermodynamic stability of hydrogen interstitials in $BaZrO_3$ perovskite oxide from density functional calculations, Faraday Discuss. 134 (2007) 247-265.

[7] H. Iwahara, T Yajima, T. Hibino, K. Ozaki and H. Suzuki, Protonic conduction in calcium, strontium and barium zirconates**,** Solid State Ionics 61 (1993) 65-69.

[8] T. Norby, Solid-state protonic conductors: principles, properties, progress and prospects, Solid State Ionics 125 (1999) 1-11.

[9] K.D. Kreuer, Proton-conducting oxides, Annu. Rev. Mater. Res 33 (2003) 333-359.

[10] A.R. Akbarzadeh, I. Kornev, C. Malibert, L. Bellaiche and J.M. Kiat, Combined theoretical and experimental study of the low-temperature properties of $BaZrO_3$, Phys. Rev. B. 72 (2005) 205104 (1-8).

[11] J.W. Bennett, I. Grinberg, and A.M. Rappe, Effect of symmetry lowering on the dielectric response of BaZrO3, Phys. Rev. B 73 (2006) 180102 (1-4).

[12] A. Bilić, Ground state structure of $BaZrO_3$: A comparative first-principles study, Phys. Rev. B 79 (2009) 174107 (1-9).

[13] D. Nuzhnyy, J. Petzelt, M. Savinov, T. Ostapchuk, V. Bovtun, M. Kempa, J. Hlinka, V. Buscaglia, M.T. Buscaglia, and P. Nanni, Broadband dielectric response of $Ba(Zr,Ti)O_3$ ceramics: From incipient via relaxor and diffuse up to classical ferroelectric behavior, to classical ferroelectric behavior, Phys. Rev. B 86 (2012) 014106 (1-9).

[14] M.A. Helal, T. Mori, and S. Kojima, Softening of infrared-active mode of perovskite $BaZrO_3$ proved by terahertz time-domain spectroscopy, Appl. Phys. Letter. 106 (2015) 182904 (1-4).

[15] A. Yamanaka, M. Kataoka, Y. Inabe, K. Inoue, B. Hehlen and E. Courtens, Evidence for competing orderings in strontium titanate from hyper-Raman scattering spectroscopy, Europhys. Lett. 50(5) (2000) 688-694.

[16] R.P. Lowndes and A. Rastogi, Stabilization of the paraelectric phase of $KTaO_3$ and $SrTiO_3$ by strong quartic anharmonicity, J. Phys. C: Solid State Phys. 6 (1973) 932-944.

[17] V. Goian, S. Kamba, J. Hlinka, P. Vaněk, A.A. Belik, T. Kolodiazhnyi and J. Petzelt, Polar phonon mixing in magnetoelectric $EuTiO_3$, Eur. Phys. J. B 71 (2009) 429-433.

[18] I.-S. Kim, M. Itoh, and T. Nakamura, Electrical conductivity and metal-nonmetal transition in the perovskite-related layered system $Ca_{n+1}Ti_nO_{3n+1-\delta}$ (n = 2, 3, and ∞), J. Solid State Chem. 101 (1992) 77-86.

[19] T. Kolodiazhnyi, P. Pulphol, W. Vittayakorn, N. Vittayakorn, Giant suppression of dielectric loss in $BaZrO_3$, J. Eur. Ceram. Soc. 39(14) (2019) (4144-4148).

[20] L. Levin, T.G. Amos, S.M. Bell, L. Farber, T.A. Vanderah, R.S. Roth, B.H. Toby, Phase equilibria, crystal structures, and dielectric anomaly in the $BaZrO_3$-$CaZrO_3$ system, J. Solid State Chem. 175 (2003) (170-181).

[21] H. Stetson and B. Schwartz, Dielectric properties of zirconates, J. Am. Ceram. Soc. 44(8) (1961) (420-421).

[22] E.A. Popova, E.A. Rumyantseva, B.Kh. Khananov, V.G. Zalessky, S.V. Krivovichev and S.G. Lushnikov, Anomalous behavior of the dielectric response of quantum paraelectric $CaTiO_3$ with iron impurities, JETP Letters 102(8) (2015) 530-535.

[23] K.D. Kreuer, On the development of proton conducting materials for technological applications, Solid State Ionics 97 (1997) 1-15.

[24] T. Norby and Y Larring, Concentration and transport of protons in oxides, Curr. Opin. Solid State Mater. Sci. 2 (1997) 593-599.

[25] D. Han, K. Shinoda, S. Sato, M. Majima and Y. Uda, Correlation between electroconductive and structural properties of proton conductive acceptor-doped barium zirconate, J Mater Chem A. 3 (2015) 1243-1250.

[26] B. Salce, J.L. Gravil and L.A. Boatner, Disorder and thermal transport in undoped $KTaO_3$, J. Phys.: Condens. Matter 6 (1994) 4077-4092.

[27] O. Bidault, M. Maglione, M. Actis and M. Kchikech, Polaronic relaxation in perovskites, Phys. Rev. B. 52(6) (1995) (4191-4197).

[28] E. Iguchi and K.J. Lee, Dielectric relaxations in $SrTiO_3$ doped with La_2O_3 and MnO_2 at low temperatures, J. Mater. Sci. 28 (1993) (5809-5813).

[29] A. Tkach, P. M. Vilarinho and A. L. Kholkin, Dependence of dielectric properties of manganese-doped strontium titanate ceramics on sintering atmosphere, Acta Mater. 54 (2006) 5385-5391.

[30] M. Valant, T. Kolodiazhnyi, A.K. Axelsson, G.S. Babu and N.M. Alford, Spin ordering in Mn-doped $KTaO_3$?, Chem Mater. 22 (2010) 1952-1954.

[31] T. Kolodiazhnyi, Origin of extrinsic dielectric loss in 1:2 ordered, single-phase $BaMg_{1/3}Ta_{2/3}O_3$, J Eur Ceram Soc. 43 (2014) 1741-1753.

[32] F. Borsa, U.T. Hochli, V.D. Klink and D. Rytz, Condensation of random-dielectric dipoles: Li in $KTaO_3$, Phys Rev Lett. 45 (1980) 1884-1887.

[33] E. Iguchi, N. Kubota, T. Nakamori, N. Yamamoto and K.J. Lee, Polaronic conduction in n-type $BaTiO_3$ doped with La_2O_3 or Gd_2O_3, Phys. Rev. B 43(10) (1991) 8646-8649.

[34] M. Swift, A. Janotti, Small polarons and point defects in barium cerate, Phys. Rev. B 92 214114 (2015).

[35] H.G. Bohn and T. Schober, Electrical conductivity of the high-temperature proton conductor $BaZr_{0.9}Y_{0.1}O_{2.95}$, J. Am. Ceram. Soc. 83(4) (2000) 768–772.

[36] W. Wang and A.V. Virkar, Ionic and electron–hole conduction in $BaZr_{0.93}Y_{0.07}O_{3-\delta}$ by 4-probe dc measurements, J. Power Sources 142 (2005) 1-9.

[37] A. Lindman, P. Erhart, and G. Wahnström, Polaronic contributions to oxidation and hole conductivity in acceptor-doped $BaZrO_3$, Phys. Rev. B 94 (2016) 075204-(1-9).

[38] L. Mazzei, A. Perrichon, A. Mancini, G. Wahnström, L. Malavasi, S.F. Parker, L. Börjesson and M. Karlsson, Local structure and vibrational dynamics in indium-doped barium zirconate, J. Mater. Chem. A 7 (2019), 7360-7372.

[39] I. Oikawa and H. Takamura, Correlation among oxygen vacancies, protonic defects, and the acceptor dopant in Sc-doped $BaZrO_3$ studied by 45Sc nuclear magnetic resonance, Chem. Mater. 27(19) (2015), 6660–6667.

[40] M. Karlsson, A. Matic, D. Engberg, M.E. Björketun, M. M. Koza, I. Ahmed, G. Wahnström, L. Börjesson and S.-G. Eriksson, Quasielastic neutron scattering of hydrated $BaZr_{0.90}A_{0.10}O_{2.95}$ (A=Y and Sc), Solid State Ionics 180 (2009) 22–28.

[41] P.G. Sundell, M.E. Björketun, and G. Wahnström, Density-functional calculations of prefactors and activation energies for H diffusion in $BaZrO_3$, Phys. Rev. B 76 (2007) 094301 (1-7).

Figure captions

Fig 1. X-ray patterns from the powder XRD of undoped $BaZrO_3$ (2N, 3N and 4N) and doped-BaZrO3 (1% and 2%Sc) sintered in air at 1650˚C for 20.

Figure 2 The microstructure of as-sintered (a) BZ 2N, (b) BZ 3N (c) BZ 4N, (d) 1%Sc-doped BZ and (e) 2%Sc-doped BZ. All samples were sintered at 1650˚C for 20 hours in air.

Fig 3. Dielectric permittivity and tan δ of $BaZrO_3$ (2N, 3N and 4N) sintered in air at 1650˚C for 20 hours and measured at 1 kHz from 2 K to 360 K (a). Frequency dependence of dielectric permittivity and tan δ measured from 2 K to 100 K of BZ 3N (b).

Fig 4. Temperature dependence of tan δ of BZ 2N, 3N and 4N ceramics measured at different frequencies (a), Low-temperature tan δ dependence of the same samples measured at 2-200 K (b).

Fig 5. Low temperature dielectric loss of 1% and 2%Sc-doped $BaZrO_3$ sintered in air (black solid dots) and annealed in Ar (red solid triangles) (a). The dielectric permittivity and tan δ of 1% and 2%Sc-doped $BaZrO_3$ sintered in air (b). The four peaks are labeled as T_1, T_2, T_3 and T_4, respectively.

Fig 6. Low temperature dielectric loss of undoped-$BaZrO_3$ (2N, 3N and 4N) sintered in air (black solid dots) and annealed in Ar (red solid triangles) (a). Arrhenius plot of frequency dependence of dielectric peaks T_1, T_2, T_3 and T_4 (b).

Fig 7. Temperature dependence of tan δ measured from 300 K to 680 K of $BaZrO_3$ 4N (a) and 1%Sc-doped $BaZrO_3$ (b) at various frequencies.

Fig 8. Arrhenius plot of frequency dependence of dielectric loss peak of $BaZrO_3$ (2N, 3N and 4N) and Sc-doped $BaZrO_3$ (1% and 2%Sc) measured from 300 K to 680 K.

Fig 9. Temperature dependence of dielectric permittivity and tan δ of $BaZr_{0.98}Sc_{0.009}Nb_{0.011}O_3$ sintered in air at various frequencies.

Fig 10. %Weight change of $BaZr_{0.98}Sc_{0.02}O_3$ and $BaZr_{0.98}Sc_{0.009}Nb_{0.011}O_3$ determined from thermogravimetric analysis (TGA).

Table 1. The unit cell size and unit cell volume for undoped $BaZrO_3$ and acceptor-doped (1% and 2%Sc) $BaZrO_3$.

System	***a* (Å)**	**Volume (Å)^3**
$BaZrO_3$ 2N	4.19420(3)	73.7814(4)
$BaZrO_3$ 3N	4.19406(3)	73.7741(5)
$BaZrO_3$ 4N	4.19444(2)	73.7943(4)
1%Sc	4.19447(2)	73.7959(4)
2%Sc	4.19445(2)	73.7946(4)

Table 2 Activation energies of pure $BaZrO_3$ of different purities sintered in air and annealed in Ar.

System	Sintered in air		Annealed in Ar	
	$E_{a(LT)}$ **(eV)**	f_0 $(\times 10^{10})$ **(Hz)**	$E_{a(LT)}$ **(eV)**	f_0 $(\times 10^{10})$ **(Hz)**
$BaZrO_3$ 2N	0.025(1)	3.2(6)	0.025(1)	3.5(2)
	0.043(1)	17.4(9)	-	-
	0.066(4)	0.4(4)	0.069(1)	0.9(5)
	0.215(3)	20.3(5)	0.276(8)	0.02(1)
$BaZrO_3$ 3N	0.024(1)	1.4(9)	0.025(4)	2.8(9)
	0.044(8)	0.2(8)	0.044(1)	0.3(1)
$BaZrO_3$ 4N	0.016(6)	1.8(1)	0.016(7)	3.1(2)
	-	-	0.026(6)	6.1(2)
	0.047(9)	0.6(2)	0.050(3)	0.01(2)
	0.067(1)	0.5(1)	0.069(1)	0.7(3)

Table 3 Low temperature activation energies and f_0 parameter of Sc-doped $BaZrO_3$ sintered in air and annealed in Ar.

System	**Sintered in air**		**Annealed in Ar**	
	$E_{a(LT)}$ (eV)	f_0 ($\times 10^{10}$) **(Hz)**	**$E_{a(LT)}$ (eV)**	f_0 ($\times 10^{10}$) **(Hz)**
1%Sc	0.026(1)	5.4(20)	0.026(1)	4.6(4)
	0.057(2)/0.03(2)	0.03(1)/0.0002(1)	-	-
	0.117(2)	0.4(1)	-	-
	0.175(2)	5.7(1)	-	-
2%Sc	0.031(1)	10.5(7)	0.028(1)	2.6(2)
	0.060(4)/0.026(3)	0.04(3)/0.0001(9)	-	-
	0.122(2)	0.8(2)	-	-
	0.175(2)	5.7(1)	-	-

Table 4 High temperature activation energies and f_0 parameter of undoped- and doped-$BaZrO_3$ sintered in air.

System	Sintered in air	
	$E_{a(HT)}$ (eV)	f_0 ($\times 10^{10}$) **(Hz)**
$BaZrO_3$ 2N	0.82(3)	10.7(6)
$BaZrO_3$ 3N	0.59(3)	0.3(3)
$BaZrO_3$ 4N	0.75(2)	0.4(2)
1%Sc	0.54(1)	1.2(5)
2%Sc	0.53(5)	1.1(2)

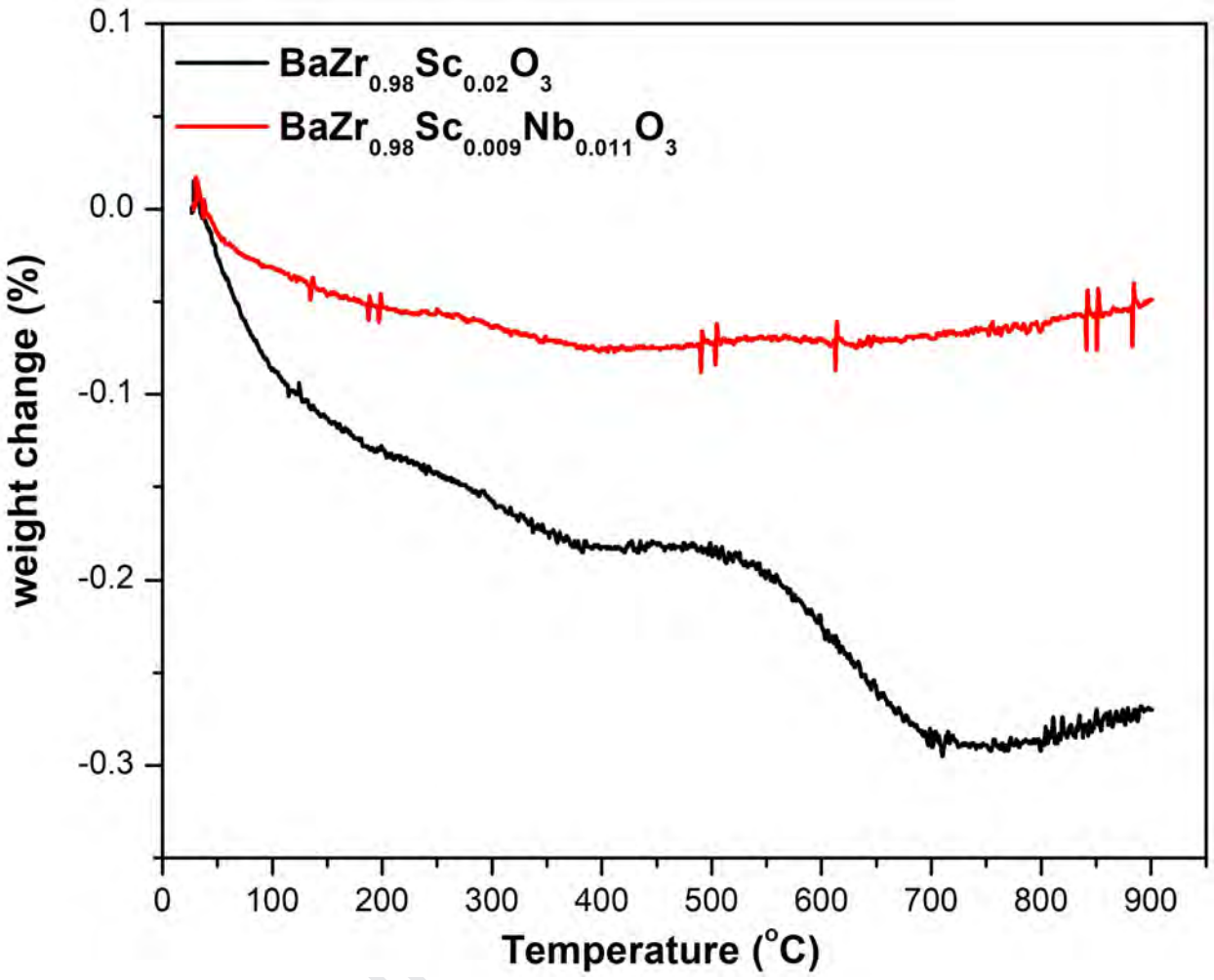
BaZr0.98Sc0.02O3
BaZr0.98Sc0.009Nb0.011O3
weight change (%)
0.1
0.0
-0.1
-0.2
-0.3
0
100
200
300
400
500
600
700
800
900
Temperature (°C)

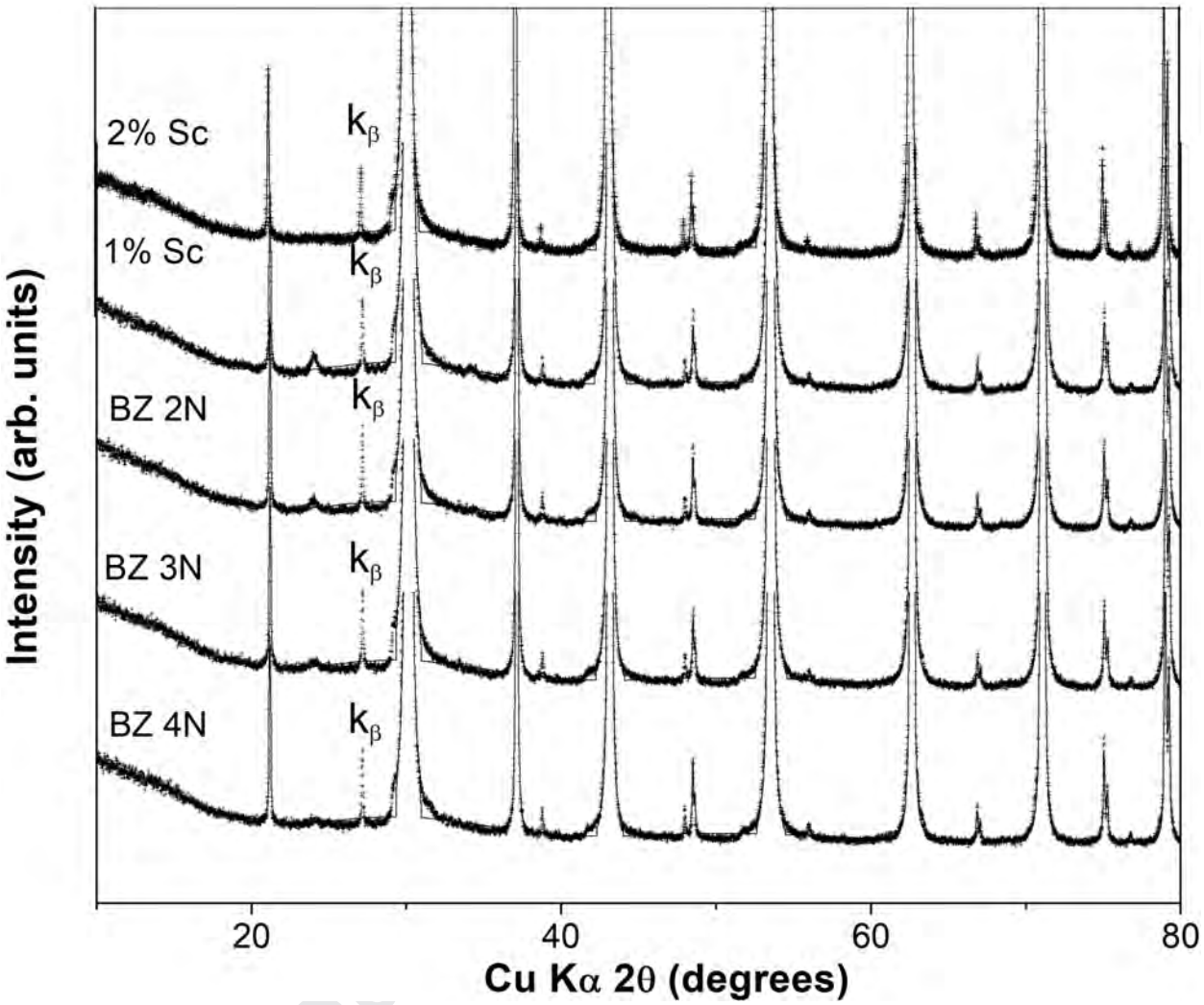
2% Sc
1% Sc
BZ 2N
BZ 3N
BZ 4N
k_β
Intensity (arb. units)
20
40
60
80
Cu Kα 2θ (degrees)

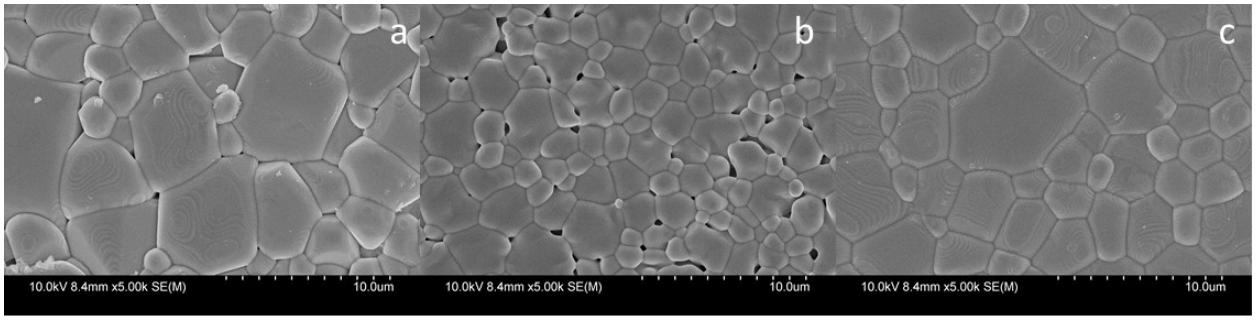

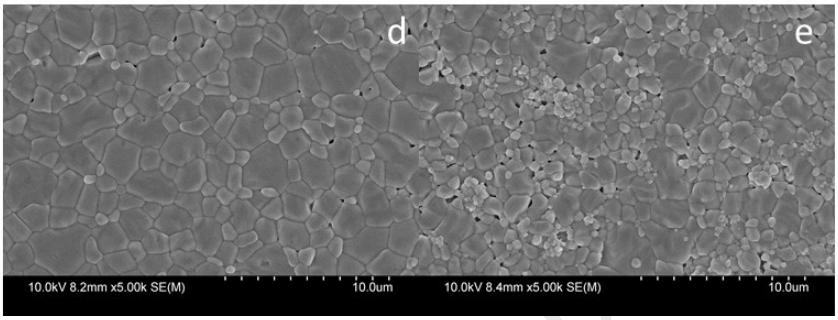

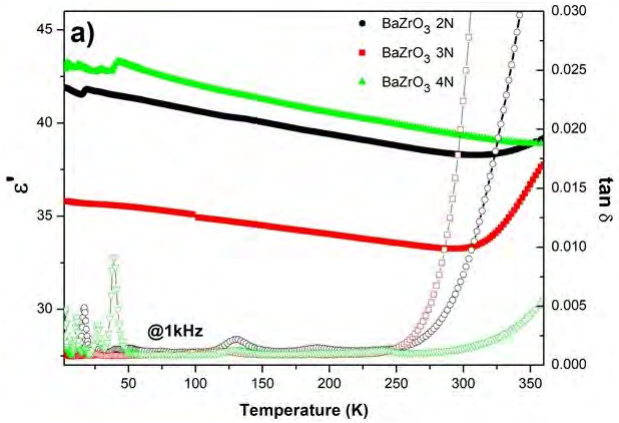

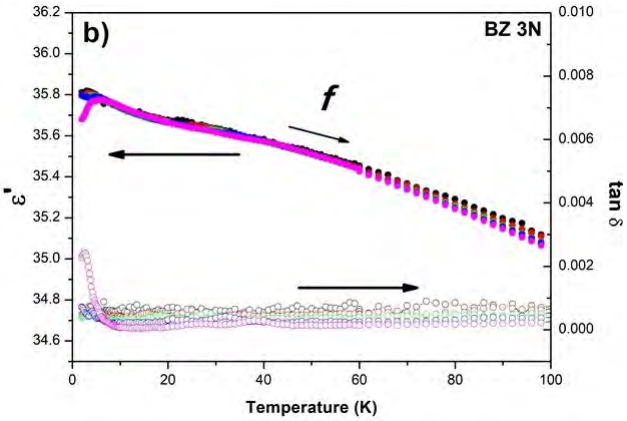

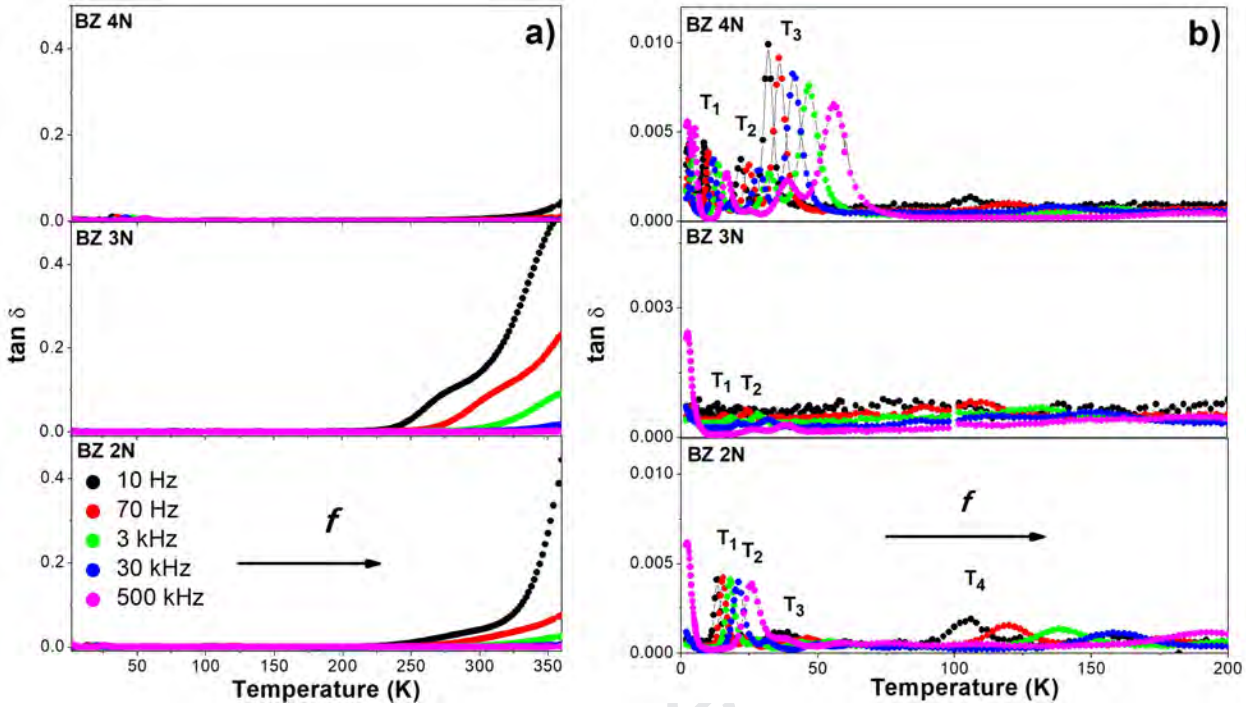

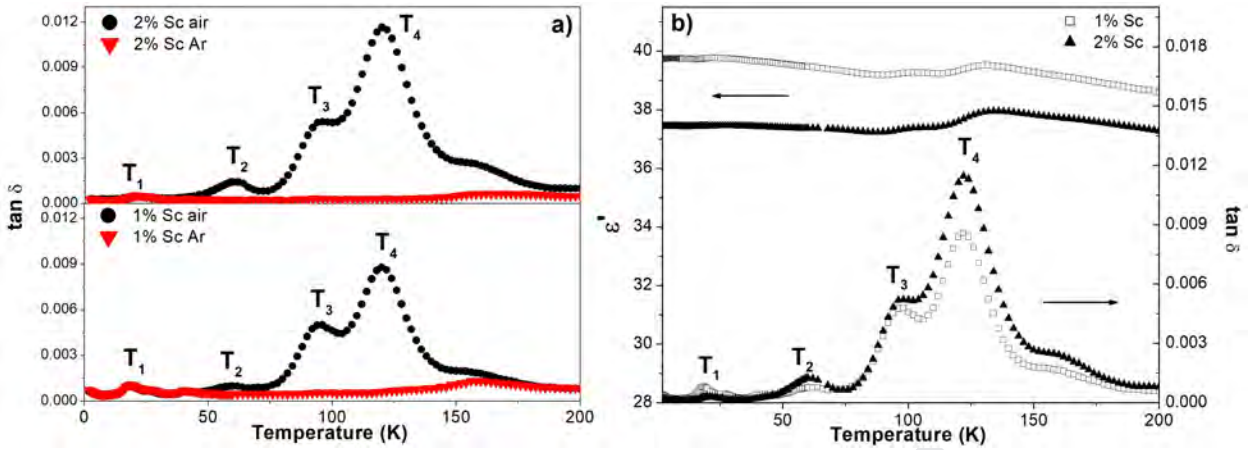

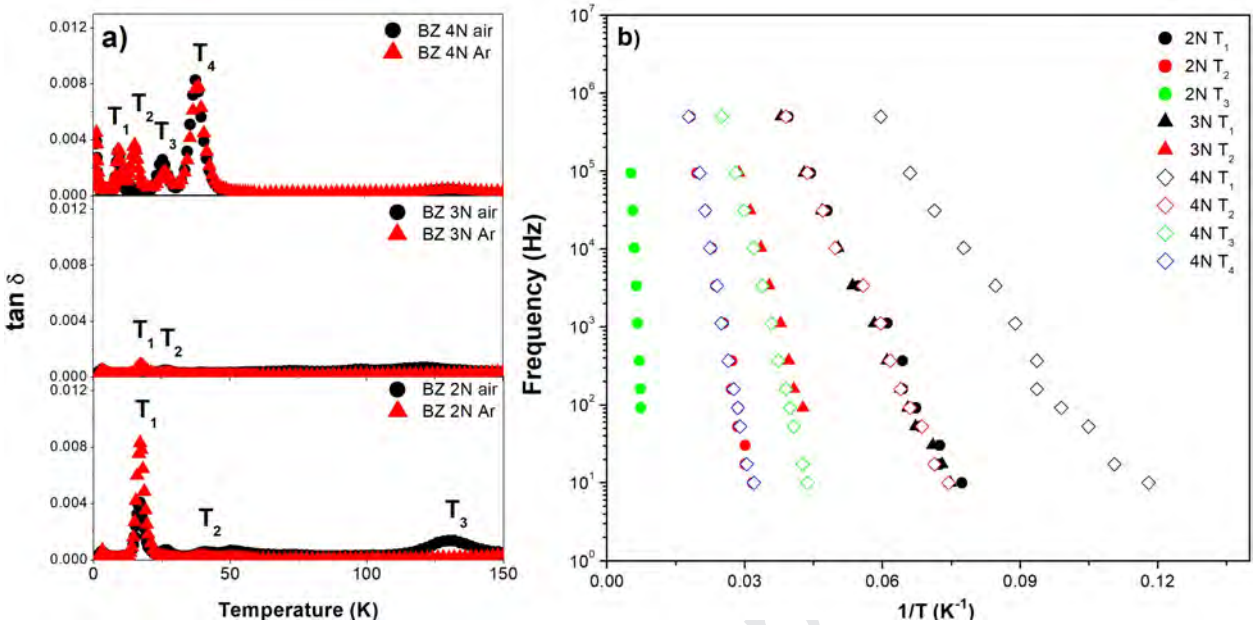

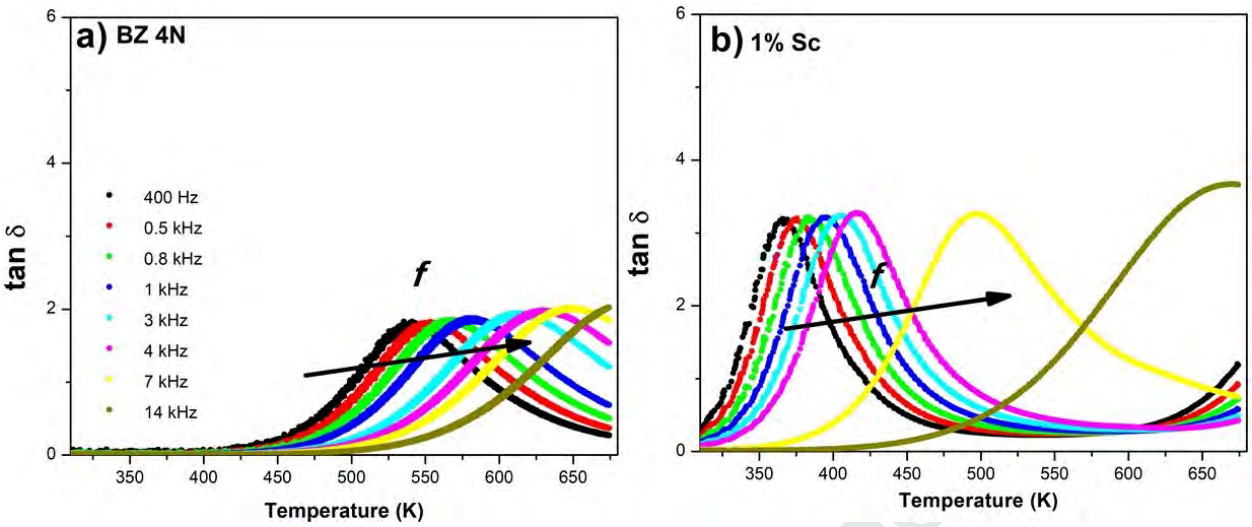

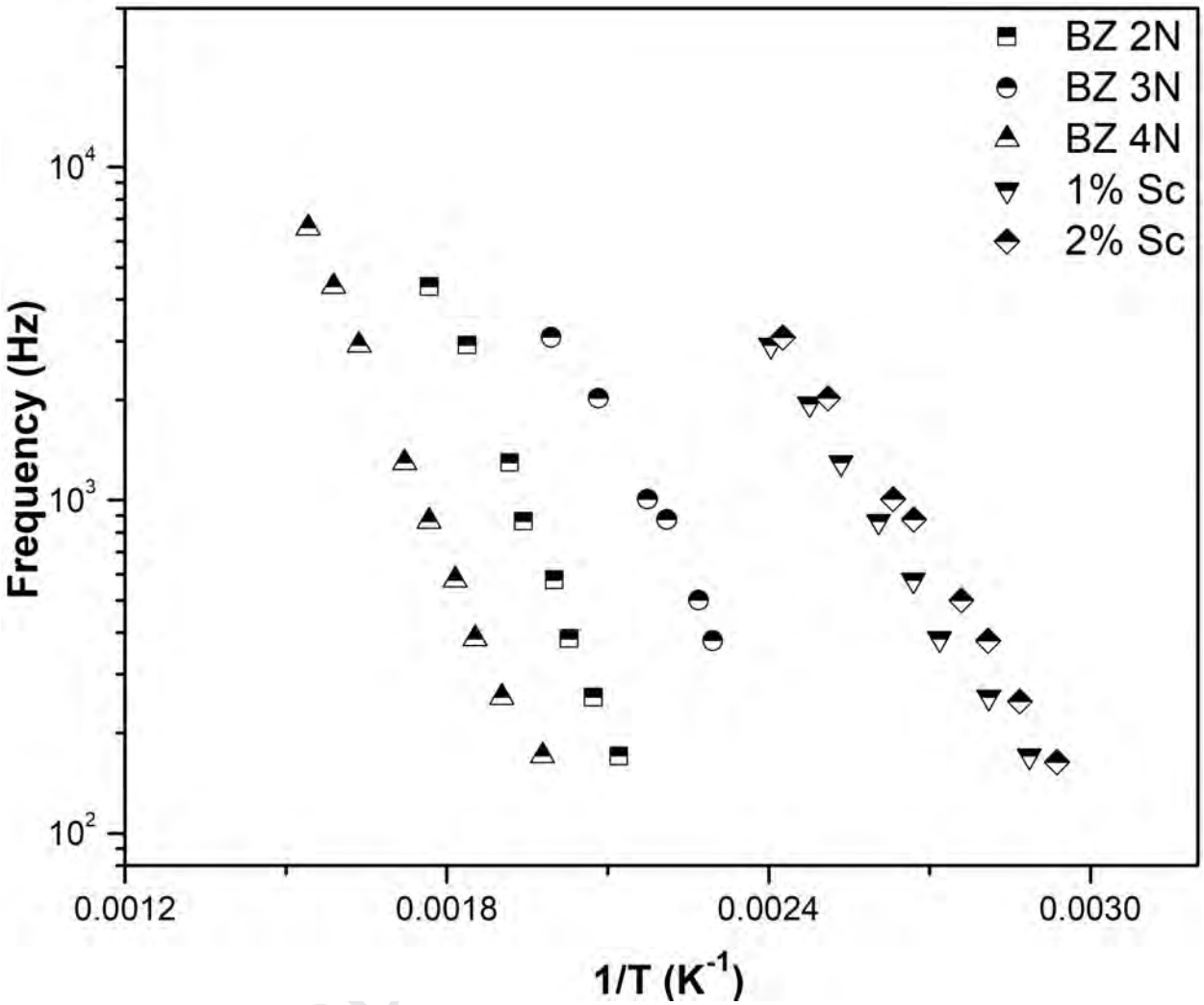
BZ 2N
BZ 3N
BZ 4N
1% Sc
2% Sc
Frequency (Hz)
10^4
10^3
10^2
0.0012
0.0018
0.0024
0.0030
1/T (K^{-1})

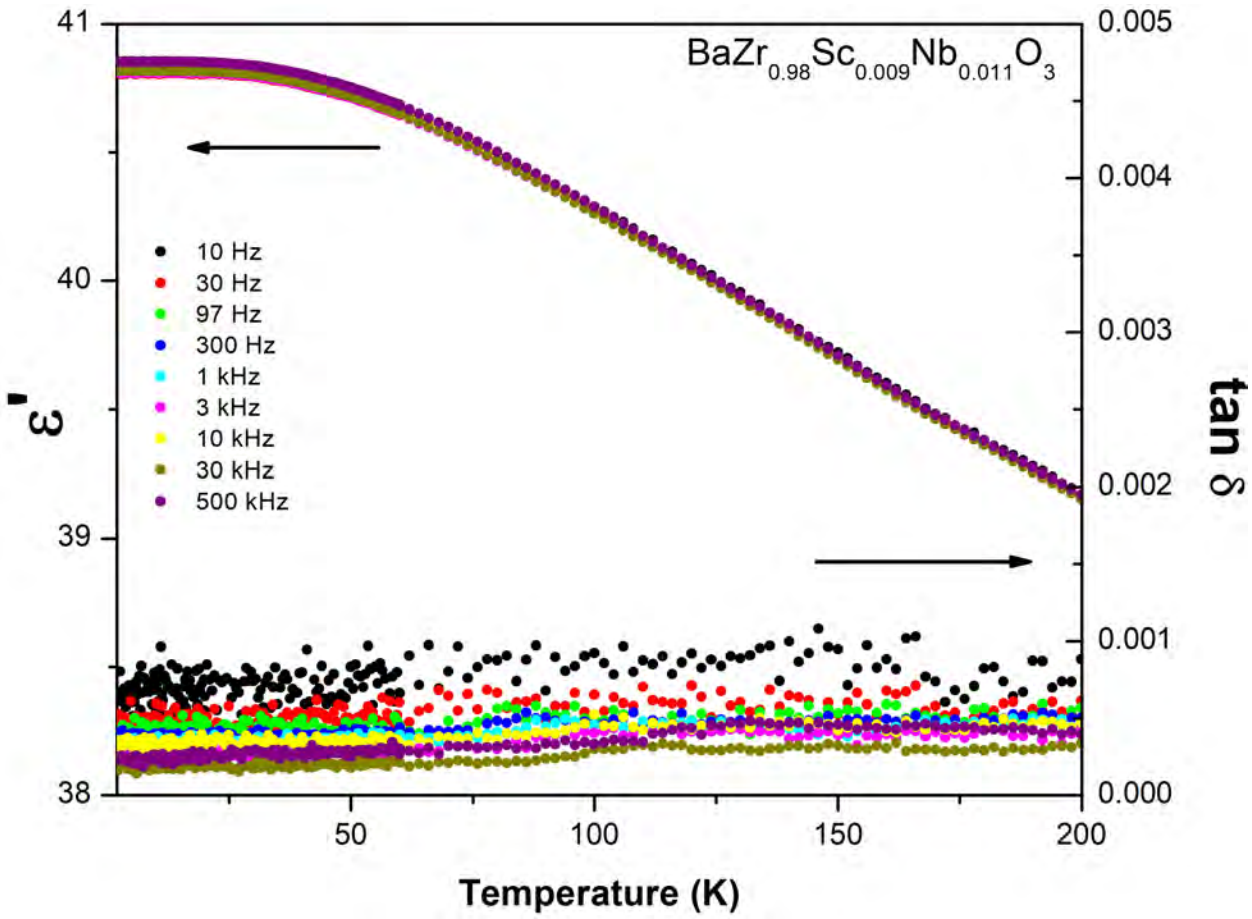
BaZr0.98Sc0.009Nb0.011O3
10 Hz
30 Hz
97 Hz
300 Hz
1 kHz
3 kHz
10 kHz
30 kHz
500 kHz
ε'
tan δ
Temperature (K)
41
40
39
38
0.005
0.004
0.003
0.002
0.001
0.000
50
100
150
200

“The authors declare that there are no conflicts of interest regarding the publication of this paper”